# Quantitative parameters of primary roughness for describing the morphology of surface discontinuities at various scales

Tikou Belem[*]

*Université du Québec en Abitibi-Témiscamingue (UQAT), Research Institute in Mining and Environment (RIME), 445, boul. de l'Université, Rouyn-Noranda, Quebec, J9X 5E4 Canada*

**Abstract.**   In this paper, five different quantitative parameters were proposed for the characterization of the primary roughness which is the component of surface morphology that prevails during large strike-slip faults of more than 50 m. These parameters are mostly the anisotropic properties of rock surface morphology at various scales: (i) coefficient ($k_a$) and degree ($\delta_a$) of apparent structural anisotropy of surface; (ii) coefficient ($k_r$) and degree ($\delta_r$) of real structural anisotropy of surface; (iii) surface anisotropy function $P(\varphi)$; and (iv) degree of surface waviness ($W_s$). The coefficient and degree of apparent structural anisotropy allow qualifying the anisotropy/isotropy of a discontinuity according to a classification into four classes: anisotropic, moderately anisotropic/isotropic and isotropic. The coefficient and degree of real structural anisotropy of surface captures directly the actual surface anisotropy using geostatistical method. The anisotropy function predicts directional geometric properties of a surface of discontinuity from measurements in two orthogonal directions. These predicted data may subsequently be used to highlight the anisotropy/isotropy of the surface (radar plot). The degree of surface waviness allows qualifying the undulation of anisotropic surfaces. The proposed quantitative parameters allows their application at both lab and field scales.

**Keywords:**   rock joint; surface roughness; anisotropy; geostatistical method; waviness

## 1. Introduction

In the literature, most of the experimental studies for modeling the mechanical behavior of rock joints are carried out on various types of artificial joints (rocks and mortars). The morphology of these joints has been in saw teeth, irregular triangles, a combination of various triangles, undulations, etc. (e.g., Hong *et al*. 2014). But a closer look shows that the common point between these surfaces is their anisotropy (Belem *et al*. 2000, 2007, Chen *et al*. 2016, Ge *et al*. 2015). Indeed, all these surfaces present distinct structures (or characteristics) along *x* and *y* directions (regular or irregular geometry) which will involve necessarily a different mechanical behavior according to *x* and *y* directions (e.g., Grasselli 2006, Zang *et al*. 2014). It can be anticipated that a single parameter does not sufficiently characterize the morphology which includes characteristics such as amplitude (surface point elevations), angularity and geometric texture (asperity slopes and angles), waviness (periodicity), anisotropy, and, in a less pronounced way, curvature (Belem *et al*. 2000, Barbosa 2009, Tatone and Grasselli 2010, Chen *et al*. 2016, Pickering and Aydin 2015).

---

∗Corresponding author, Professor, E-mail: Tikou.Belem@UQAT.ca

It is common practice to obtain rock fracture properties by performing laboratory testing (Fathi *et al.* 2016, Park and Song 2013, Nemoto *et al.* 2009, Karami and Stead 2008, Grasselli 2006, Fardin *et al.* 2001) on samples of smaller fractures having limited size (e.g., 100-400 mm). This may or may not be a sufficient size to reach the "stationarity threshold" of even the smaller fractures, as surface roughness is scale-dependent (Rasouli and Harrison 2000, Fardin *et al.* 2001, Fardin 2008). According to Jing (2003), there is an acute lack of understanding of the hydro-mechanical behavior of large fractures (such as faults and fracture zones) with a large width (e.g., 10 mm-50 m). Consequently, there is a lack of proper constitutive models for large fracture zones, which in turn reduces our current capacity to develop numerical models for large-scale problems (Jing 2003). There is usually uncertainty concerning scaling experimental results to field application (use of empirical methods). The strong correlation between roughness, aperture and hydro-mechanical properties of a single rock joint, such as stiffness, shear strength and transmissivity, requires the development of descriptive models and quantitative parameters to describe roughness (Grasselli *et al.* 2002, Belem *et al.* 2000), waviness and aperture (Lanaro 2000, Marache *et al.* 2002, Sharifzadeh *et al.* 2006).

As an alternative, new laser-based 3D high resolution scanners have recently been developed to measure large-scale fracture surface roughness over scales of 10 $\mu$m to 120 m (Feng *et al.* 2003, Renard *et al.* 2006, Sagy *et al.* 2007, Lato *et al.* 2007, 2009, Barbosa 2009, Bitenc *et al.* 2014, 2015). Exposed fault surface data provided the first quantitative evidence that fault-surface roughness evolves with increasing slip. It has been observed that small-slip faults (slip < 1 m) are rougher than large-slip faults (slip 10-100 m or more) parallel to the slip direction (Sagy *et al.* 2007). These authors also observed that surfaces of small-slip faults have asperities over the entire range of observed scales, while large-slip fault surfaces are polished at small scale but have undulating structure at scales of a few to several meters. Thus, at scales of 1-2 m parallel to the slip, the roughness of large-slip faults is about one order of magnitude smoother than that of small-slip faults.

These observations have at least two implications: (i) both joint surface primary (waviness) and secondary (asperities) roughness components must be taken into account in modeling sliding or shearing distances up to 1 m. Indeed, a relationship was observed by Sagy *et al.* (2007) between laboratory and field data for small-slip faults (slip < 1 m), since the power spectra measured by the lab profilometer and field LiDAR (Light detection and ranging) follow a similar trend (continuity). This continuity across five orders of magnitude demonstrates at the same time the consistency of the two different measurement tools; (ii) over shearing distances up to 10 m, only surface primary roughness prevails (waviness), and must be taken into account in joint characterization. At this large scale, the power spectra measured by the lab profilometer and field LiDAR for large-slip faults do not connect across scales (Sagy *et al.* 2007).
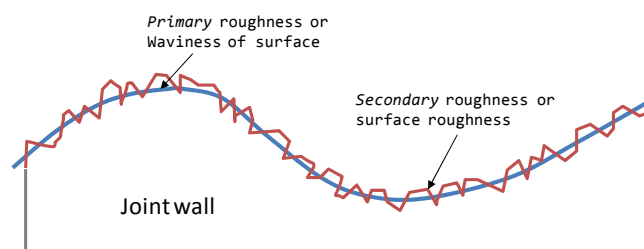


Fig. 1 Joint surface morphology waviness (1st order) and asperities (2nd order) components

The surface morphology can be subdivided into two main components (Kana *et al*. 1996): the secondary or second-order roughness (i.e., asperities component) and the primary or first-order roughness (i.e., waviness component). The asperities are defined by the surface heights distribution (which correspond to the *sensu stricto* roughness) while the primary roughness is defined by the overall surface texture geometry (which describe the surface anisotropy). Fig. 1 is an illustration of the two different components of surface texture (asperities and waviness).

The main objective of the research is to characterize the primary roughness in terms of (i) apparent "structural anisotropy" of surface; (ii) real "structural anisotropy" of surface; (iii) anisotropy function; and (iv) waviness of the surface.


## 2. Quantitative description of the surfaces primary roughness

The apparent structural anisotropy will be described using linear/directional geometrical parameters while the real structural anisotropy will be described by means of geostatistical analysis (autocorrelation function) based on surface 3D profilometric data (e.g., Belem *et al*. 2000, 2007, Belem and Homand 2002).

### 2.1 Coefficient of apparent structural anisotropy of surface

The surface linear/directional geometric parameters calculated along both *x* direction (0° or 180°) and *y* direction (90° or 270°) can be used to well describe an apparent structural anisotropy of surface morphology with regard to either *x*- and *y*-axis or (*x*, *y*) plane. The coefficient of apparent structural anisotropy of surface morphology $k_a$ was previously defined (Belem *et al*. 2000) as the ratio of the half-minor axis *b* and the half-major axis *a* of apparent anisotropy ellipse given as follows

$$k_a = \frac{\text{minor axis } b}{\text{major axis } a} = \frac{\min\left\{(Parameter)_{x,y}\right\}}{\max\left\{(Parameter)_{x,y}\right\}} = \frac{\min\left\{\overline{\theta}_{p(x,y)}\right\}}{\max\left\{\overline{\theta}_{p(x,y)}\right\}} \qquad 0 \le k_a \le 1 \tag{1}$$

where $\theta_{p(x,y)}$ is the weighted mean angle calculated along the *x*-axis or *y*-axis (directional angle).

For evenly spaced surface morphological data with a constant step $\Delta s$ along the *s*-axis (*s* stand for *x* or *y*), the weighted mean angle of the inclinations of the roughness linear profiles $\theta_{p(x,y)}$ (0° $\le \theta_{p(x,y)} < 90°$) is given in the discrete form as follows (Belem *et al*. 2000)

$$\left(\overline{\theta}_p\right)_{s=x,y} = \text{atan}\left(\sum_{j=1}^{M_s} L_s^j \left(\frac{1}{N_s^j - 1}\sum_{i=1}^{N_s^j-1}\left|\frac{z_{i+1}-z_i}{\Delta s}\right|\right)\middle/ \sum_{j=1}^{M_s} L_s^j\right) \tag{2}$$

where $M_s$ = total number of profiles in *s*-direction (*x*-axis or *y*-axis); $z_i$ = algebraic values of asperity heights along the roughness linear profile; $\Delta s$ = sampling step along *s*-axis; $N_s^j$ = number of discrete points corresponding to the *j*[th] profile along *s*-direction (*x*-axis or *y*-axis); $L_s^j$ = length of the *j*[th] profile along *s*-direction (*x*-axis or *y*-axis). For a given joint surface, if all roughness profiles have equal length $L_s$, then Eq. (2) gives an arithmetic mean. However, if the roughness profiles have different lengths, then Eq. (2) gives a weighted mean.
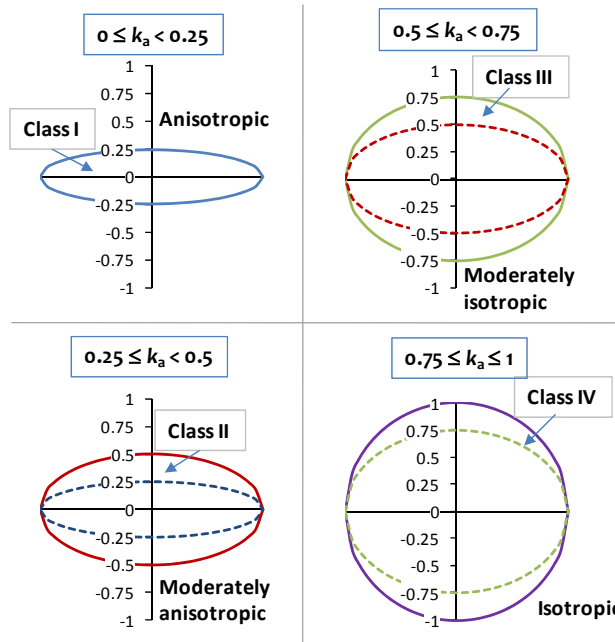
Fig. 2 Schematic illustration of apparent anisotropy ellipses based on $k_a$ values



(a) Joing surface roughness
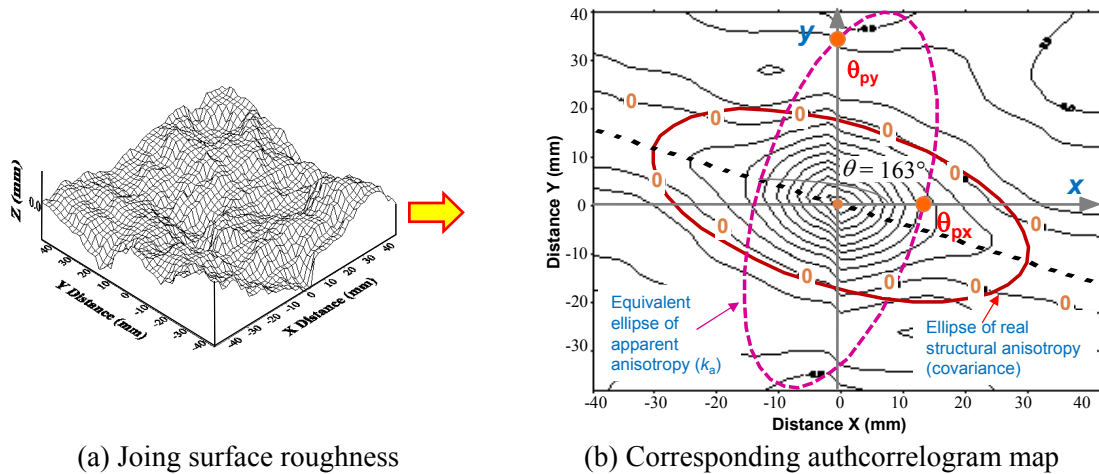(b) Corresponding authcorrelogram map

Fig. 3 Illustration of the real and apparent structural anisotropy: (a) joint surface; (b) corresponding 2D auto-correlogram map and the ellipses of real (solid line) and apparent (dotted line) structural anisotropy

It should be noted that $k_a$ may well be equally calculated using $Z2$ parameter ($Z2_x$ and $Z2_y$) and other linear geometric parameters. Parameter $k_a$ exclusively quantifies apparent structural anisotropy of surface with respect to the $x$- and $y$-axis of a test sample and any deviation from this coordinates system is not taken into account in Eq. (1). When $k_a = 0$, the surface morphology is considered anisotropic (e.g., saw-tooth and corrugated surfaces, etc.); when $k_a = 1$ the surface morphology is considered isotropic. Apparent structural anisotropy of surface morphology was

arbitrarily subdivided into four classes: class I, II, III and IV. Fig. 2 illustrates these four classes and their description. Note that the orientation of the ellipses is for illustration only.

A real anisotropic surface having a major principal axis oriented at 45° regarding *x*-axis or *y*-axis will give $k_a = 1$ ($\theta_{p(y)} = \theta_{p(x)}$) indicating an erroneous isotropic surface (see Fig. 3). Consequently, the limitations of the $k_a$ parameter make it better suited for the characterization of man-made or numerically generated artificial anisotropic joint surfaces (saw-tooth, corrugated, etc.) because it is insufficient for real structural anisotropy analysis (Belem *et al*. 2007). In general however, rock joint samples are sheared along the *x* or *y* directions (only multiaxial shearing machines can shear a joint sample along an intermediate direction). Even if the *x* direction supporting the joint shearing differed from the minor or major principal axis of real structural anisotropy, the semi-quantitative $k_a$ parameter would have no significant impact. Indeed, based on the above assumption, the principal direction of the real anisotropy should be perpendicular to the one fitted to the weighted mean angles $\theta_{p(y)}$ and $\theta_{p(x)}$ which define $k_a$. Consequently, the apparent anisotropy is related indirectly to the real structural anisotropy of the surface (Fig. 3).

### 2.2 Degree of apparent structural anisotropy of surface

The easiest way to quantify the apparent anisotropy of surface is to have a parameter which value will be 0% when the surface is not anisotropic (i.e., isotropic) and 100% when the surface is perfectly anisotropic. From the already defined coefficient of apparent anisotropy $k_a$, the degree of apparent anisotropy $\delta_a$ can be defined as follows

$$\delta_a(\%) = 100 \times (1 - k_a) \qquad 0\% \leq \delta_a \leq 100\% \tag{3}$$

Table 1 presents the range of variation of $k_a$ and $\delta_a$ for the four classes of anisotropy. Table 2 summarizes the calculation of linear angularity parameters, the coefficient ($k_a$) and the degree ($\delta_a$) of surface apparent structural anisotropy and the surface primary roughness for three different rock joint surfaces.

### 2.3 Degree of real structural anisotropy of surface

The geostatistical analysis showed that the correlation distance *d*c of the correlogram quantify the influence zone limit of the analyzed structure. Consequently, knowing the values of *d*c in all directions allows characterizing the real structural anisotropy of a surface discontinuity. Rather than calculating directional 1D correlograms, it is preferable to obtain a map representation (iso-value contours) of the correlations $\rho$ (2D auto-correlograms or "auto-correlomap") given as follows

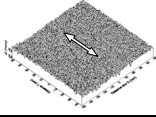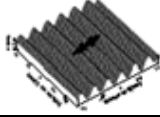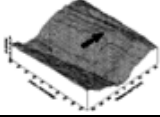Table 1 Classification of apparent structural anisotropy of surface

| Class of anisotropy | Range of coefficient $k_a$ | Range of degree $\delta_a$ | Description |
|---|---|---|---|
| Class I | $0 \leq k_a < 0.25$ | $100\% \leq \delta_a < 75\%$ | Anisotropic |
| Class II | $0.25 \leq k_a < 0.5$ | $75\% \leq \delta_a < 50\%$ | Moderately anisotropic |
| Class III | $0.5 \leq k_a < 0.75$ | $50\% \leq \delta_a < 25\%$ | Moderately isotropic |
| Class IV | $0.75 \leq k_a \leq 1$ | $25\% \leq \delta_a \leq 0\%$ | Isotropic |

$$\rho(h_x, h_y) = \dfrac{\dfrac{1}{(M-h_x)(N-h_y)}\displaystyle\sum_{j=1}^{M-h_x}\sum_{k=1}^{N-h_y}\left(Z_{j,k}-\overline{Z}\right)\left(Z_{j+h_x,k+h_y}-\overline{Z}\right)}{\dfrac{1}{MN}\displaystyle\sum_{j=1}^{M}\sum_{k=1}^{N}\left(Z_{j,k}-\overline{Z}\right)^2} \tag{4}$$

where $MN$ is the total number of data points on the surface, $M\text{-}h_x$ and $N\text{-}h_y$ are the number of pairs of data points respectively at a lag distance $h_x \in [-M/2; M/2]$ and $h_y \in [-N/2; N/2]$, $Z_{j,k}$ is the random variable representing the surface heights $z(x, y)$.

An elliptic shape of the iso-contours indicates a mean anisotropy, while a circular shape of the iso-contours indicates a mean isotropy (see Figs. 3(b)-4). The principal direction of real structural anisotropy $\beta$ corresponds to the ellipse lengthening direction highlighted by the 2D auto-correlogram and therefore to the mean direction of the surface geometric texture. Considering for example a corrugated surface, that results in the fact that this principal direction $\beta$ is on average parallel to the orientation of the peak of the undulations. For such surfaces, it's therefore expected to have higher values of angularity parameters along the transverse direction to the principal direction of anisotropy (see Fig. 3).

Table 2 Calculated parameters for three different surfaces roughness

| | Hammered surface | Corrugated surface | Rough surface |
|---|---|---|---|
| 3D morphology |  |  |  |
| $\overline{\theta}_{p(x)}$ ($\varphi = 0°$ or $180°$) | 8.73° | 10.27° | 10.18° |
| $\overline{\theta}_{p(y)}$ ($\varphi = 90°$ or $270°$) | 8.76° | 6.17° | 7.16° |
| $\overline{\theta}_{p(xy)}$ ($\varphi = 45°$) | 8.78° | 2.16° | 4.38° |
| Apparent anisotropy $k_a$ | 0.99 | 0.21 | 0.43 |
| $k_a$ classification | Class IV (isotropic) | Class I (anisotropic) | Class II (moderately anisotropic) |
| $\delta_a = 100\times(1-k_a)$ (%) | 0.6% | 79.0% | 57.0% |
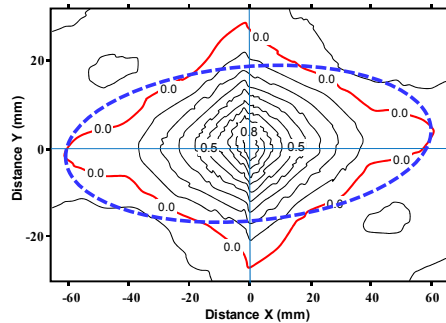


(a) 2D autocorrelogram



$$R = \sqrt{(X_R)^2 + (Y_R)^2} = a$$

$$r = \sqrt{(X_r)^2 + (Y_r)^2} = b$$

$$\beta = \tan^{-1}\left(\frac{Y_R}{X_R}\right)$$
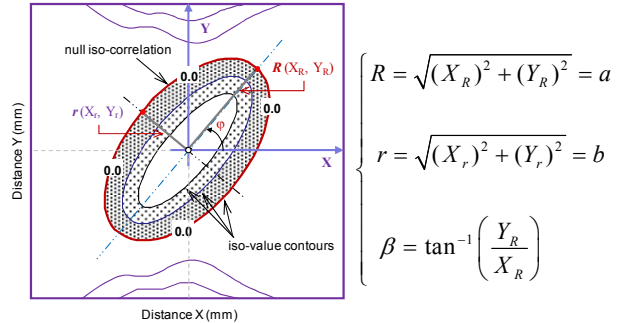
(b) Idalized 2D autocorrelogram

Fig. 4 Schematic illustration of the anisotropy ellipses based on the 2D auto-correlogram

It should be emphasized that the 2D auto-correlogram (Fig. 4) highlights the spatial organization of the texture forming the geometry of surface, while the angularity parameters describes the geometry of the asperities (roughness). From Fig. 4 the half-major axis $R$ and the half-minor axis $r$ can be used to define the degree of real structural anisotropy of surface $\delta_r$ which is given as follows

$$\delta_r = \frac{R-r}{r} = \left( \frac{\sqrt{X_R^2 + Y_R^2}}{\sqrt{X_r^2 + Y_r^2}} - 1 \right) = \frac{R}{r} - 1 \qquad 0 \leq \delta_r \leq \delta_{r\_max} \qquad (5)$$

When $\delta_r = 0$ the ellipse is reduced to a circle ($R = r$) and the surface is no longer anisotropic but rather perfectly isotropic. The surface start to exhibit anisotropic structure from $\delta_r = 1$ ($R = 2r$) to $\delta_r = \delta_{r\_max}$ ($R > 2r$). It is clear that $\delta_{r\_max}$ value depends on the ellipse axis ratio which may be as high as 6 ($R = 6r$). When the surface is anisotropic, the principal direction of real structural anisotropy of the joint surface $\beta = \tan^{-1}(Y_R/X_R)$ as shown in Fig. 3.

## 2.4 Alternative definition of the degree of real structural anisotropy of surface

Even if the method of fitting an ellipse of anisotropy to the null iso-correlation is rigorous and relevant, it remains mostly manual and laborious, unless a specific algorithm can be developed for this purpose. Indeed, the autocorrelation map can be obtained using for example the commercial software Surfer® and then manually fit the ellipse to the null iso-correlation but this step could be better performed using a specific automatic processing algorithm.

An alternative method of direct calculation of $\delta_r$ can then be found for overcoming these difficulties. Indeed, polar sections spaced at constant angle across the 2D auto-correlogram can be used to obtain different 1D correlograms in these directions (Fig. 5(a)). From these polar sections, when the surface is structurally isotropic, all 1D correlograms must give a single value of correlation distance dc. On the contrary, if the surface is anisotropic different values of $dc$ must be obtained and consequently lower and upper limits can be found: $dc_{min}$ and $dc_{max}$. From Fig. 5(b) and the known upper ($dc_{max}$) and lower ($dc_{min}$) limits of the correlation distance $dc$, the degree of real structural anisotropy of surface can be defined as follows

$$\delta_r = \frac{dc_{max} - dc_{min}}{dc_{min}} = \frac{dc_{max}}{dc_{min}} - 1 \qquad 0 \leq \delta_r \leq \delta_{r\_max} \qquad (6)$$

In Eq. (6), when $\delta_r = 0$ ($dc_{max} = dc_{min} = dc$) the joint surface is perfectly isotropic. When $\delta_r = 1$ the surface starts to become anisotropic and $dc_{max} = 2dc_{min}$. This version of $\delta_r$ is easier to calculate than the one given by Eq. (5).

## 2.5 Proposed anisotropy function

Usually, the calculation of various 2D parameters is done only with regard to $x$- and $y$-axis. Therefore, it would be interesting to predict the value of these parameters for any direction, $\varphi$. As previously argued, it is clear that surface real structural anisotropy can be well described by an ellipse of anisotropy. Knowing the three parameters describing this ellipse (half-major axis $R$, half-minor axis $r$ and the principal direction of anisotropy $\beta$) it can be interesting to express or calibrate the weighted mean angularity parameters $\theta_{p(x)}$ ($= P_x = P_{0°/180°}$) and $\theta_{p(y)}$ ($= P_y = P_{90°/270°}$) with the
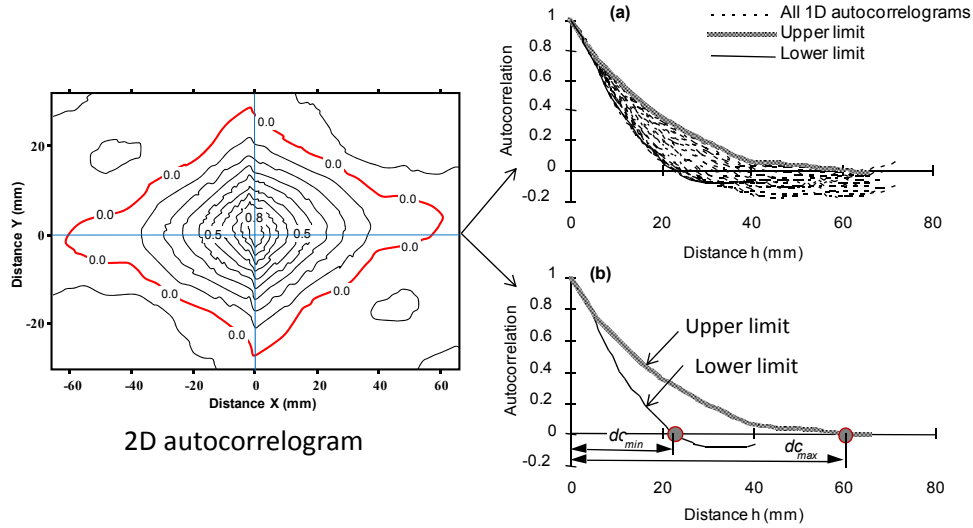
Fig. 5 1-D correlograms: (a) all polar section profiles; (b) lower and upper limit of the correlation distance $dc$

ellipse of structural anisotropy of surface. An alternative method based on geostatistical variographic analysis was recently proposed by Chen *et al.* (2016).

Let $\mathbf{E_1}$ be the ellipse of real structural anisotropy of surface determined from 2D autocorrelogram. Assuming that the principal direction associated with $\min\{\theta_{p(x,y)}\}$ is in "average" related to the principal direction of real anisotropy of surface, it is considered that the ellipse of apparent anisotropy of surface $\mathbf{E_2}$ for 2D geometric parameters is perpendicular to $\mathbf{E_1}$. The calibration of 2D geometric parameters can be done on the ellipse of apparent anisotropy from which the value of each geometric parameter $P$ along any direction $\varphi$ can be obtained using a proposed anisotropy function $P(\varphi)$ which general form is given as follows

$$P(\varphi) = P_{0°/180°} \cdot \cos^2(\varphi) + P_{90°/270°} \cdot \sin^2(\varphi) \tag{7}$$

where the initial parameters $P_x$ and $P_y$ correspond to the angularity calculated with respect to the $x$-axis ($\varphi = 0°$ or $180°$) and $y$-axis ($\varphi = 90°$ or $270°$), that is to say $P_x = P_{0°/180°}$ and $P_y = P_{90°/270°}$.

A similar approach was previously adopted by Aydan *et al.* (1996) who proposed an anisotropy function without any link to an ellipse of anisotropy. The general form of their proposed anisotropy function $F(\varphi)$ for predicting the angularity parameters of any class of surface anisotropy in any direction $\varphi$ is given as follows

$$F(\varphi) = a_1 \cos(\varphi) + b_1 \sin(\varphi) + a_2 \cos^2(\varphi) + b_2 \sin^2(\varphi) \tag{8}$$

where $a_1 = (F_{0°} - F_{180°})/2$, $b_1 = (F_{90°} - F_{270°})/2$, $a_2 = (F_{0°} + F_{180°})/2$, $b_2 = (F_{90°} + F_{270°})/2$. Constants $a_1$ and $b_1$ will always vanish for angularity parameters not taking into account "+" and "−" angles, so that Eq. (8) will be reduced to Eq. (7).

An equivalent anisotropy function was earlier proposed by Wong (1985) and is given as follows

$$Z(\varphi) = Z_{0°} + (Z_{90°} - Z_{0°})\sin^2(\varphi) \qquad (9)$$

Note that these two equations give similar results to those obtained using Eq. (7). Fig. 6 presents a comparison of these three anisotropic functions for three different types of surface morphology. It can be observed first of all that these three functions predict exactly the same angle values. It further notes that these functions perfectly predict the calculated angle values for two anisotropic surfaces (Figs. 6(b)-(c)), while the prediction becomes less good for an isotropic surface (Fig. 6(a)). The measured angles are given in Table 2. Beside each graph is shown the ellipse of apparent anisotropy of the surface and its corresponding classification.

The importance of structural anisotropy function (Eq. (7)) surface is that it predicts the geometrical parameters in directions ranging from 0° to 360° from only two geometric parameters calculated in two orthogonal directions. Subsequently, a polar representation (or radar) of these geometrical parameters will show if the surface is anisotropic or isotropic. Fig. 7 is a polar representation of the weighted mean angularity parameter $\overline{\theta}_{p(x,y)}$ of the three surfaces which
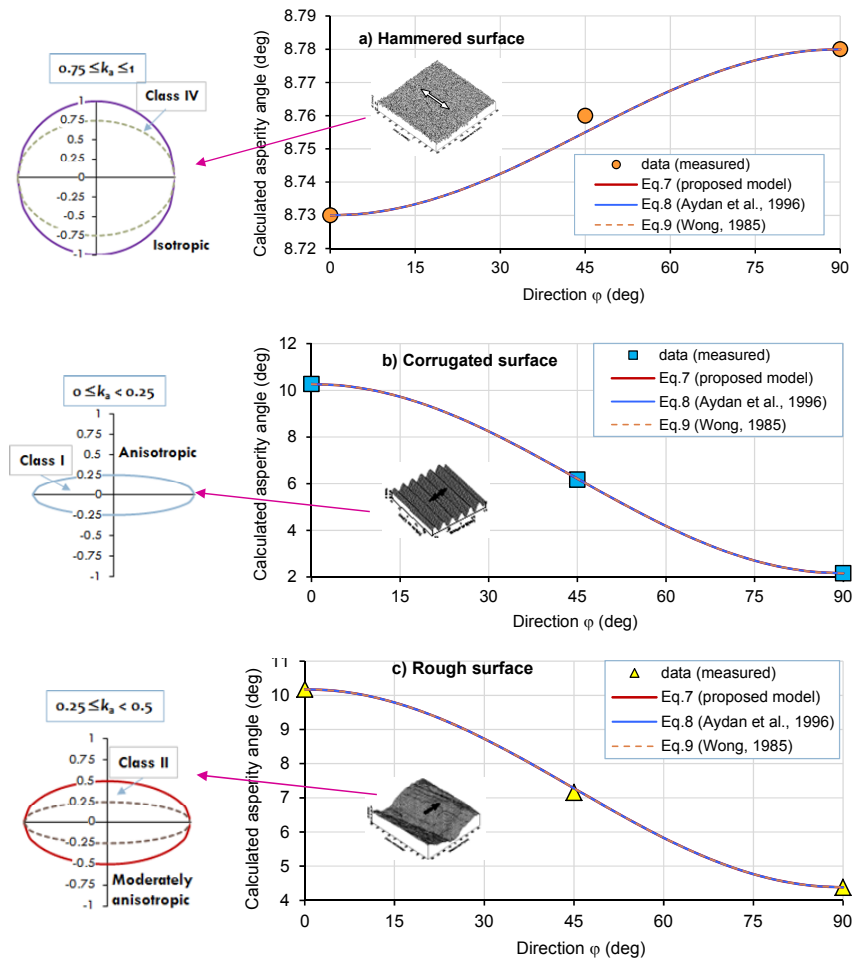


Fig. 6 Comparison of predicted mean angles using the anisotropy functions and for three different surfaces

**a) Hammered surface**



**b) Corrugated surface**
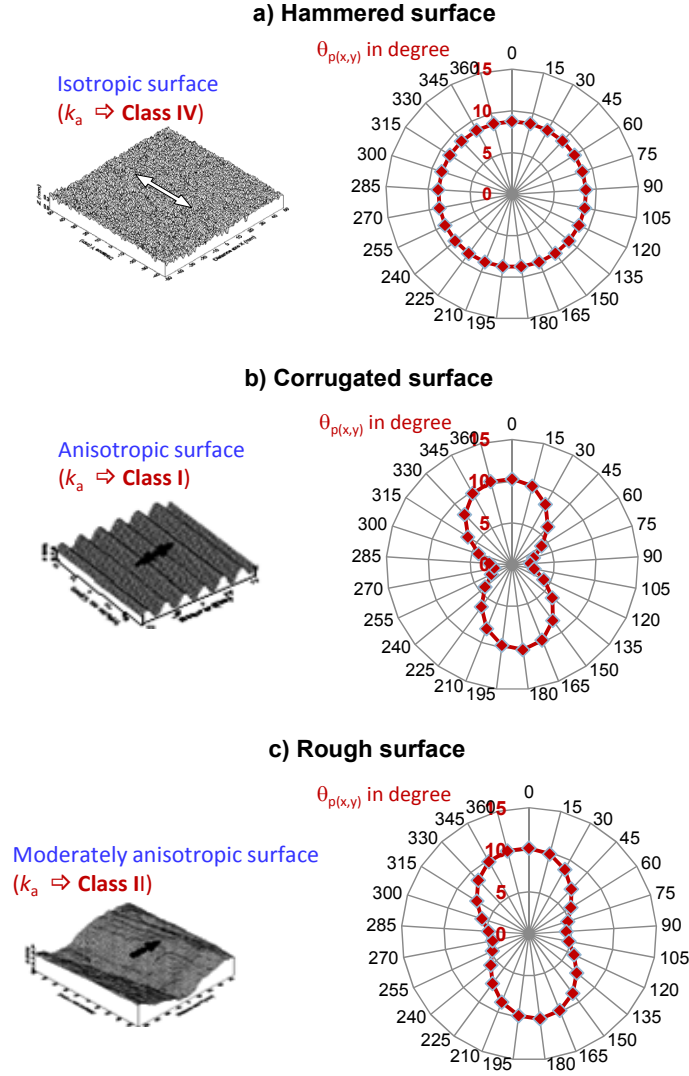


**c) Rough surface**



Fig. 7 Polar representation of the weighted mean angularity parameter $\theta_{p(x,y)}$ for the three surfaces

geometrical characteristics are given in Table 2. This figure confirms exactly the qualification of surfaces made on the basis of the parameter $k_a$ and its corresponding classification (see Table 1).

## 2.6 Degree of surface waviness

Any undulating/corrugated surface can be fully described by their mean amplitude $a_m$, and wavelength or period $\lambda_x$ along the $x$-axis and $\lambda_y$ the wavelength or period along the $y$-axis (see Fig. 8). If the maximum amplitude of a surface is $a_0$ then the mean amplitude of this surface $a_m$ is half $a_0$ ($a_m = a_0/2$).
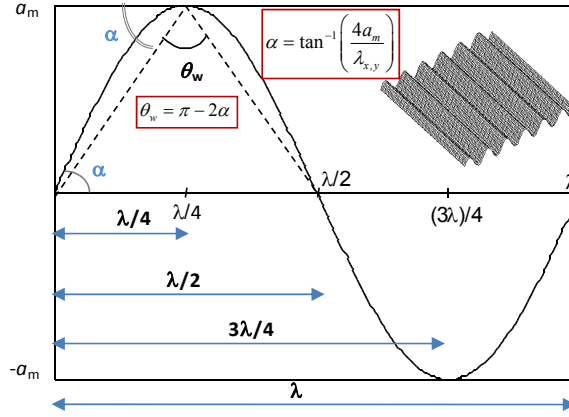
Fig. 8 Parameters describing a sinusoid linear profile of one wavelength

From Fig. 8 the angle $\theta_w$ is the wrinkle angle (or ripple angle) of a corrugated surface and $\alpha$ the angle of the dotted triangle with the horizontal are calculated as follows

$$\theta_w = \pi - 2\alpha \tag{10}$$

Let $\omega$ be the undulation index; the angle of the dotted triangle $\alpha$ is given as follows

$$\omega = \frac{4a_m}{\lambda_{x,y}} = \frac{2a_0}{\lambda_{x,y}} \quad \text{and} \quad \alpha = \tan^{-1}(\omega) \tag{11}$$

From Eqs. (10) and (11) the degree of surface waviness $W_s$ can be defined as follows

$$W_s(\%) = \frac{\pi - \theta_w}{\pi} = \frac{\pi - (\pi - 2\alpha)}{\pi} = \left(\frac{2\alpha}{\pi}\right) = \frac{2}{\pi}\tan^{-1}\left(\frac{2a_0}{\lambda_{x,y}}\right) \times 100 \quad \text{with} \quad 0\% \le W_s < 100\% \tag{12}$$

Eq. (12) shows that when $W_s = 0\%$ the surface is perfectly flat and smooth and therefore non-corrugated. When $W_s$ tends towards 100% ($Ws \rightarrow 100$) the surface undulations look like "needles" or sticks (and will look like to an isotropic structure surface). Even if this parameter is intended for anisotropic corrugated surfaces, it can still be used for all types of surface. In that case the waviness should be viewed as in average.

A parametric study done by the author has shown that for a perfectly isotropic surface, the correlation distance $dc \approx \lambda_{x,y}/2$ (or $\lambda_{x,y} \approx 2dc$), while for anisotropic surfaces, $dc \approx \lambda_{x,y}/4$ (or $\lambda_{x,y} \approx 4dc$). A general relationship between the wavelength $\lambda_{x,y}$ and the correlation distance $dc$ can thus be drawn as: $\lambda_{x,y} \approx n \cdot dc$, where $n$ is the real structural anisotropy index ($n = 2$ for isotropic surfaces and $n = 4$ for anisotropic surfaces). Substituting $\lambda_{x,y} \approx n \cdot dc$ in Eq. (12) yield

$$W_s(\%) = 2 \cdot \pi^{-1} \cdot \tan^{-1}\left(\frac{2a_0}{n \cdot dc}\right) \times 100 \quad \text{with} \quad 0\% \le W_s < 100\% \tag{13}$$

As might well be expected, it is possible to propose an alternative classification of real structural anisotropy of surface based on the $\lambda_{x,y}/dc$ ratio ($= n$). Indeed, it is possible to match the four classes of surface anisotropy defined using $k_a$ parameter (see Table 1) with the following subdivision values of $n$: Class IV ($2 \leq n \leq 2.5$ for isotropic surface), Class III ($2.5 \leq n < 3$ for moderately isotropic surface), Class II ($3 \leq n < 3.5$ for moderately anisotropic surface), and Class I ($3.5 \leq n < 4$ for anisotropic surface). From this new classification system it is now possible to define the actual structural anisotropy of surface coefficient $k_r$ as follows

$$k_r = \left( \frac{n_{anisotropy} - n}{n_{isotropy}} \right) = \frac{4-n}{2} = 2\left( 1 - \frac{n}{4} \right) \qquad \text{with} \quad 0 \leq k_r \leq 1 \tag{14}$$

From Eq. (14) the practical way of defining the degree of real structural anisotropy of surface $\delta_r$ (see Eqs. (5) and (6)) is as follows

$$\delta_r(\%) = 100 \times \left( 1 - k_r \right) \qquad 0\% \leq \delta_r \leq 100\% \tag{15}$$

For a given class of anisotropy, Eq. (14) allows to match parameter $n$ (real structural anisotropy index) to the apparent structural anisotropy coefficient $k_a$ using the following equation

$$k_r = \left( 2 - \frac{n}{2} \right) = k_a \qquad \rightarrow n = 2\left( 2 - k_a \right) = 2\left( 2 - k_r \right) \tag{16}$$

Substituting Eq. (16) into Eq. (12) yields the dependency of the degree of surface waviness on the apparent structural anisotropy coefficient $k_a$ as follows

$$W_s(\%) = 2 \cdot \pi^{-1} \cdot \tan^{-1}\left( \frac{a_0}{(2-k_a)dc} \right) \times 100 \qquad \text{with} \quad 0\% \leq W_s < 100\% \tag{17}$$

It can clearly be seen that Eq. (17) actually reflects the scale of the surface discontinuity by taking into account the surface anisotropy ($k_a$, $k_r$), the maximum amplitude $a_0$ and the correlation distance $dc$ that can be obtained directly from 3D topographic data and the 2D auto-correlogram calculation using commercial software such as Surfer® from Golden Software.

Table 3 shows the correspondence between $n$ (real anisotropy index) and $k_r$ (real structural anisotropy coefficient). It should be emphasized, however, that this classification is also arbitrary.

Table 3 Alternative classification of real anisotropy of surface based on $\lambda_{x,y}/dc$ ratio ($= n$)

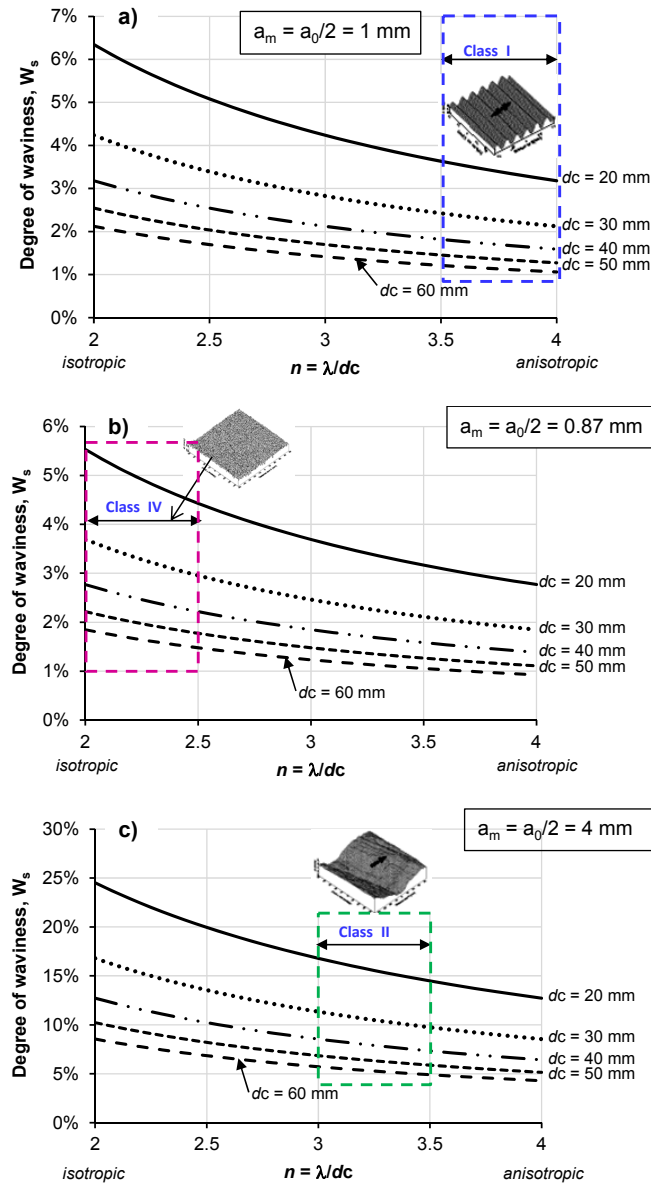| Class of anisotropy | Range of $n$ | Range of $k_r$ | Description |
|---|---|---|---|
| Class IV | $2 \leq n \leq 2.5$ | $0.75 \leq k_r \leq 1$ | Isotropic |
| Class III | $2.5 \leq n < 3$ | $0.5 \leq k_r < 0.75$ | Moderately isotropic |
| Class II | $3 \leq n < 3.5$ | $0.25 \leq k_r < 0.5$ | Moderately anisotropic |
| Class I | $3.5 \leq n < 4$ | $0 \leq k_r < 0.25$ | Anisotropic |

Fig. 9 Variation in wavelength-to-correlation distance ratio as a function of degree of waviness: (a) for different values of $dc$ and an amplitude $a_0 = 2$ mm; (b) for different values of $dc$ and an amplitude $a_0 = 1.742$ mm; (c) for different values of $dc$ and an amplitude $a_0 = 8.103$ mm; (d) for $dc = 20$ mm and three different amplitudes $a_0 = 2$, 1.742 and 8.103 mm

Fig. 9 shows the evolution of the degree of waviness as a function of $\lambda_{x,y}/dc$ ratio ($= n$) and for different average amplitude $a_m$ (where amplitude $a_0 = 2 \cdot a_m$). It can be observed that $W_s$ (%) is proportional to $a_m$ (or $a_0$) and $dc$. Also, for $a_m$ and a given $\lambda_{x,y}/dc$ ratio ($= n$) the degree of waviness $W_s$ (%) decreases when $dc$ increases, and the undulations of the surface become more and more planar.
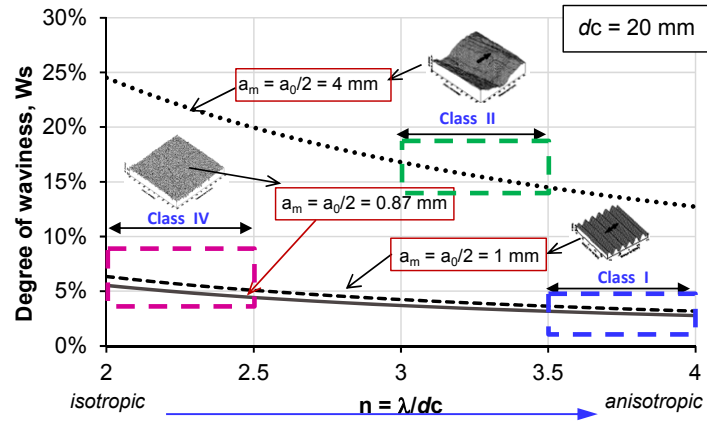
Fig. 10 Variation in wavelength-to-correlation distance ratio as a function of degree of waviness and for
$d$c = 20 mm and three different amplitudes $a_0$ = 2, 1.742 and 8.103 mm

Fig. 10 presents the evolution of the degree of waviness as a function of $\lambda_{x,y}/d$c ratio (= $n$) and for $d$c = 20 mm and different mean amplitude $a_m$ (where amplitude $a_0 = 2 \cdot a_m$). This figure shows that for a given $d$c value (e.g., $d$c = 20 mm), the degree of waviness decreases when going from an isotropic surface to an anisotropic surface regardless of the value of the mean amplitude of the surface.

## 3. Conclusions

In this paper, five quantitative parameters have been proposed for the characterization of the primary roughness of rock joint surfaces in terms of apparent "structural anisotropy" of surface, real "structural anisotropy" of surface, anisotropy function, and waviness of the surface. These parameters are needed for describing both second order roughness and primary roughness (surface undulations = anisotropy) which is prevailing at large scale shearing mechanisms. Indeed, since the roughness/morphology of surface discontinuities is scale-dependent, the proposed structural anisotropy function and the degree of surface waviness allow taking easily into account the scale effect. Also, two methods of surface anisotropy classification have been proposed, one for the apparent structural anisotropy of surface and the other for the real structural anisotropy of surface.

The calculations of these parameters rely mainly on 3D analysis of surface topography data. Since laser tools such as LiDAR or terrestrial laser scanning (TLS) have been applied for the scanning of field scale fracture surfaces, this implies that the proposed parameters can be useful and widely applicable to these large scales through parameters such as the amplitude $a_0$ and the correlation distance $d$c.

## Acknowledgments

# References

Aydan, Ö., Shimizu, Y. and Kawamoto, T. (1996), "The anisotropy of surface morphology characteristics of rock discontinuities", *Rock Mech. Rock Eng.*, **29**(1), 47-59.

Barbosa, R.E. (2009), "Constitutive model for small rock joint samples in the lab and large rock joint surfaces in the field", *Proceedings of the 3rd CANUS Rock Mechanics Symposium*, *ROCKENG09*, Toronto, Canada, May.

Belem, T. and Homand, F. (2002), "Characterization of the anisotropy of rock joints surface morphology", *Proceedings of the 2nd International Conference on New Development in Rock Mechanics*, Shenyeng, China, October.

Belem, T., Homand-Etienne, F. and Souley, M. (2000), "Quantitative parameters for rock joint surface roughness", *Rock Mech. Rock Eng.*, **33**(4), 217-242.

Belem, T., Souley, M. and Homand, F. (2007), "Modelling rock joint walls surface degradation during monotonic and cyclic shearing", *Acta Geotechnica*, **2**(4), 227-248.

Bitenc, M., Kieffer, D.S., Khoshelham, K. and Vezočnik, R. (2014), "Quantification of rock joint roughness using terrestrial laser scanning", *Proceedings of the 12th Congress of the International Association of Engineering Geology*, *Engineering Geology for Society and Territory*, Torino, Italy, September.

Bitenc, M., Kieffer, D.S., Khoshelham, K. and Vezočnik, R. (2015), "Book Chapter: Quantification of rock joint roughness using terrestrial laser scanning", In: *Engineering Geology for Society and Territory*, Springer International Publishing, Switzerland, **6**, pp. 835-838.

Chen, S.J., Zhu, W.C., Yu, Q.L. and Liu, X.G. (2016), "Characterization of anisotropy of joint surface roughness and aperture by variogram approach based on digital image processing technique", *Rock Mech . Rock Eng.*, **49**(3), 855-876.

Fardin, N. (2008), "Influence of structural non-stationarity of surface roughness on morphological characterization and mechanical deformation of rock joints", *Rock Mech. Rock Eng.*, **41**(2), 267-297.

Fardin, N., Stephansson, O. and Jing, L. (2001), "The scale dependence of rock joint surface roughness", *Int. J. Rock Mech. Mining Sci.*, **38**(5), 659-669.

Fathi, A., Moradian, Z., Rivard, P., Ballivy, G. and Boyd, A. (2016), "Geometric effect of asperities on shear mechanism of rock joints", *Rock Mech. Rock Eng.*, **49**(3), 801-820.

Feng, Q., Fardin, N., Jing, L. and Stephansson, O. (2003), "A new method for in situ non-contact roughness measurement of large rock fracture surfaces", *Rock Mech. Rock Eng.*, **36**(1), 3-25.

Ge, Y., Tang, H., Eldin, M.A.M.E., Chen, P., Wang, L. and Wang, J. (2015), "A description for rock joint roughness based on terrestrial laser scanner and image analysis", *Sci. Rep.*, **5**, 16999, pp. 1-10. DOI: 10.1038/srep16999

Grasselli, G. (2006), "Shear strength of rock joints based on quantified surface description - Manuel Rocha medal recipient", *Rock Mech. Rock Eng.*, **39**(4), 295-314.

Grasselli, G., Wirth, J. and Egger, P. (2002), "Quantitative three-dimensional description of a rough surface and parameter evolution with shearing", *Int. J. Rock Mech. Mining Sci.*, **39**(6),789-800.

Hong, E.-S., Lee, I.-M., Cho, G.-C. and Lee, S.-W. (2014), "New approach to quantifying rock joint roughness based on roughness mobilization characteristics", *KSCE J. Civ. Eng.*, **18**(4), 984-991.

Jing, L. (2003), "A review of techniques, advances and outstanding issues in numerical modelling for rock mechanics and rock engineering", *Int. J. Rock Mech. Mining Sci.*, **40**(3), 283-353.

Kana, D.D., Fox, D.J. and Hisiung, S.M. (1996), "Interlock/friction model for dynamic shear response in natural jointed rock", *Int. J. Rock Mech. Mining Sci. Geomech. Abstrs.*, **33**(4), 371-386.

Karami, A. and Stead, D. (2008), "Asperity degradation and damage in direct shear test: A hybrid FEM/DEM approach", *Rock Mech. Rock Eng.*, **41**(2), 229-266.

Lanaro, F. (2000), "A random field model for surface roughness and aperture of rock fractures", *Int. J. Rock Mech. Mining Sci.*, **37**(8), 1195-210.

Lato, M., Hutchinson, D.J., Diederichs, M.S. and Kalenchuk, K. (2007), "Evaluating block shape and block volume distributions of rock faces using LiDAR and 3DEC", *Geophys. Res. Absts. (European*

*Geosciences Union*), **9**, 1-2.

Lato, M., Hutchinson., D.J., Diederichs, M.S. and Harrap, R. (2009), "Optimization of LiDAR scanning and processing for automated structural evaluation of discontinuities in rock masses", *Int. J. Rock Mech. Mining Sci.*, **46**(1), 194-199.

Marache, A., Riss, J., Gentier, S. and Chilès, J.P. (2002), "Characterization and reconstruction of a rock fracture surface by geostatistics", *Int. J. Num. Anal. Meth. Geomech.*, **26**(9), 873-896.

Nemoto, K., Watanabe, N., Hirano, N. and Tsuchiya, N. (2009), "Direct measurement of contact area and stress dependence of anisotropic flow through rock fracture with heterogeneous aperture distribution", *Earth Planet. Sci. Lett.*, **281**(1-2), 81-87.

Park, J.W. and Song, J.J. (2013), "Numerical method for the determination of contact areas of a rock joint under normal and shear loads", *Int. J. Rock Mech. Mining Sci.*, **58**, 8-22.

Pickering, C. and Aydin, A. (2015), "Modeling roughness of rock discontinuity surfaces: a signal analysis approach", *Rock Mech. Rock Eng.*, 1-7. DOI: 10.1007/s00603-015-0870-3

Rasouli, V. and Harrison, J.P. (2000), "Scale effect, anisotropy and directionality of discontinuity surface roughness", *Proceedings of the EUROCK 2000, 14th Symposium on Rock Mechanics and Tunnel Construction*, Aachen, Germany, March.

Renard, F., Voisin, C., Marsan, D. and Schmittbuhl, J. (2006), "High resolution 3D laser scanner measurements of a strike-slip fault quantify its morphological anisotropy at all scales", *Geophys. Res. Lett.*, **33**(4), (L04305). DOI: 10.1029/2005GL025038

Sagy, A., Brodsky, E.E. and Axen, G.J. (2007), "Evolution of fault-surface roughness with slip," *Geology*, **35**(3), 283-286.

Sharifzadeh, M., Mitani, Y. and Esaki, T. (2006), "Rock joint surfaces measurement and analysis of Aperture distribution under different normal and shear loading using GIS", *Rock Mech. Rock Eng.*, **41**(2), 299-323.

Tatone, B.S.A. and Grasselli, G. (2010), "A new 2D discontinuity roughness parameter and its correlation with JRC", *Int. J. Rock Mech. Mining Sci.*, **47**(8), 1391-1400.

Wong, T.F. (1985), "Geometric probability approach to the characterization and analysis of microcracking in rocks", *Mech. Mat.*, **4**(3-4), 261-276.

Zhang, G., Karakus, M., Tang, H., Ge, Y. and Zhang, L. (2014), "A new method estimating the 2D Joint Roughness Coefficient for discontinuity surfaces in rock masses", *Int. J. Rock Mech. Mining Sci.*, **72**, 191-198.

*CC*